Localization of Damage in Progressive Hydroxychloroquine Retinopathy On and Off the Drug: Inner Versus Outer Retina, Parafovea Versus Peripheral Fovea

Luis de Sisternes,[1] Julia Hu,[2] Daniel L. Rubin,[1,3] and Michael F. Marmor[2]

[1]Department of Radiology, Stanford University, Stanford, California, United States
[2]Department of Ophthalmology, Byers Eye Institute at Stanford, Stanford University School of Medicine, Palo Alto, California, United States
[3]Department of Medicine (Biomedical Informatics), Stanford University, Stanford, California, United States

Correspondence: Michael F. Marmor, Byers Eye Institute at Stanford, 2452 Watson Court, Palo Alto, CA 94303, USA;
marmor@stanford.edu.
Daniel L. Rubin, Richard M. Lucas Center, 1201 Welch Road, Stanford, CA 94305, USA;
dlrubin@stanford.edu.

Submitted: December 26, 2014
Accepted: April 22, 2015

Citation: de Sisternes L, Hu J, Rubin DL, Marmor MF. Localization of damage in progressive hydroxychloroquine retinopathy on and off the drug: inner versus outer retina, parafovea versus peripheral fovea. *Invest Ophthalmol Vis Sci*. 2015;56:3415–3426. DOI:10.1167/iovs.14-16345

Purpose. To evaluate the relative involvement of inner and outer retina in hydroxychloroquine (HCQ) retinopathy while on the drug, and after drug cessation, using data from spectral-domain optical coherence tomography (SD-OCT).

Methods. A total of 102 SD-OCT scans were obtained from 11 patients (classified as having early, moderate, or severe stages of toxicity) over a period of 4 years after cessation of HCQ. The inner and outer retina boundaries were identified automatically to measure thickness and characterize progression topographically.

Results. The segmentation of retinal layers was verified in SD-OCT cross-sections for all eyes and scans included in this study (a total of 102 scans). Topographic analysis showed that inner retina was not involved in HCQ toxicity to any meaningful degree, either between stages of retinopathy or after the drug is stopped. The characteristic bull's eye pattern of outer macula thinning appears when comparing moderate retinopathy (before any RPE damage) to the early stage. Later damage, as toxicity evolved to a severe stage, was diffuse across most of the macula. If the drug was stopped at an early or moderate stage, progression was limited to the first year and occurred diffusely without parafoveal localization.

Conclusions. Hydroxychloroquine retinopathy primarily involves outer retina (photoreceptors). Outer retinal thinning while using HCQ initially involves the parafovea, but becomes diffuse across the macula as damage progresses or after drug cessation. When HCQ is stopped at an early or moderate stage (before RPE damage), progression seems to be limited to the first year.

Keywords: hydroxychloroquine retinopathy, toxicity, optical coherence tomography, plaquenil, progression

Hydroxychloroquine (HCQ) is toxic to the retina in proportion to daily dose and duration of use, causing a characteristic retinopathy in Caucasian patients with loss of photoreceptors and eventually RPE changes in a ring around the fovea.[1,2] The mechanism of this toxicity is unclear, as animal experiments have shown the drug can affect all retinal layers,[3] whereas the damage seen in clinical imaging is primarily to the outer retina.[4] We showed recently that HCQ retinopathy can progress even after the drug is stopped, sometimes for years, but that the degree of progression is related to the severity of retinopathy and is minimal when the toxicity is detected at early stages of damage.[5] However, that study left a number of important questions unanswered, including the relative involvement of inner and outer retina, the relative involvement of parafovea and peripheral fovea, and potential differences between progression of retinopathy while using the drug or after stopping the drug.

The present report addresses these issues and presents new results. Some previous reports have suggested mild inner retina damage during HCQ usage as observed in spectral-domain optical coherence tomography (SD-OCT) images.[6–8] However, we have identified technical limitations in a commonly used commercial ganglion cell segmentation program in SD-OCT images in the presence of focal damage to the outer retina, which led us to use an experimental pixel-by-pixel segmentation paradigm and address this issue with more accurate segmentation of the retinal layers. Previous studies of HCQ retinopathy also have focused on damage to the parafovea, whereas in this report we address the nature of damage more broadly in the macula, differentiating between damage to the center of the fovea, parafovea, and the peripheral fovea ring, as well in pixel-by-pixel topographic macula maps. We also compare patterns of macular damage between different stages of maculopathy while using HCQ to the way maculopathy progresses after cessation of HCQ.

Table. Patient Demographics

Patient Label	Sex	Age at HCQ Cessation, y	HCQ Use				
			Follow-up, mo	Daily Dose, mg/kg*	Duration, y	Cumulative Dose, mg	Cumulative Dose, g/kg*
E1	F	69	33	6.6	18.0	2628	43.7
E2	M	54	23	6.5	10.0	1460	23.8
E3	F	49	51	7.0	25.0	3650	64.2
E4	F	67	13	7.3	16.0	2336	42.8
M2	F	41	38	6.5	8.0	1168	19.0
M3	F	75	27	7.0	10.0	1460	25.0
M6	F	72	17	5.9	10.5	1533	22.5
S1	F	77	43	11.0	7.0	1022	28.0
S2	F	65	40	9.2/4.6†	22.0	2482	57.0
S4	F	58	40	7.7	10.0	1460	27.9
S7	F	67	20	8.0	18.0	2628	52.6

Patients categorized as early, moderate, and severe toxicity are labeled as E, M, and S, respectively. F, female; M, male; y, years until drug stopped.
* Dose calculated by ideal weight.
† A total of 400 mg/d for 12 years, then 200 mg/d for 10 years.

Methods

Study Dataset

The present study reports data on 11 cases of hydroxychloroquine retinopathy that were monitored for 13 to 51 months after cessation of the drug. These cases are identical, with those studied previously with clinical data,[5] although several now have a longer period of follow-up. The demographics of these patients, history of drug exposure, and follow-up period are shown in the Table. Because these cases were recognized up to 5 years previously, before new demographic data[1] showed the value of dose estimation by actual weight, the data are presented relative to ideal weight (which was measured at the time of diagnosis). Cases were categorized as early, moderate, or severe toxicity as described in previous reports,[3,5] by assessing the damage present when first diagnosed with HCQ retinopathy, using a variety of screening tests (Swedish Interactive Threshold Algorithm 10-2 visual fields, SD-OCT, fundus autofluorescence, and multifocal electroretinography). To summarize: *early* is defined as patchy ellipsoid zone damage in the parafoveal region (i.e., areas of damage with parafoveal localization, but not coalesced into a clear ring); *moderate* is defined as a clear ring (50% to 100% complete) of damage, but still without RPE involvement observed by SD-OCT, funduscopy, and/or autofluorescence; and *severe* is defined as having RPE damage (by any of the assessment techniques) in the parafoveal bull's-eye region. This patient cohort was identified before it was recognized that Asian patients may show a more peripheral pattern of retinopathy[2]; all were non-Asian except for two patients with severe cases (S1 and S4) who were Filipino and had parafoveal maculopathy as well as thinning throughout the macula.

From each patient's clinic visit, we collected SD-OCT macular scans using a Cirrus high-definition (HD) OCT instrument (Carl Zeiss Meditec, Inc., Dublin, CA, USA) in the form of "cubes" with a topographic dimension of 6×6 mm and 2-mm scan depth. The initial or baseline visit was defined as the time toxicity was detected and drug was stopped. The time interval between follow-up visits varied (as shown in the Results section) and was 17 months on average. The Cirrus instrument uses a scanning pattern with different resolution in each direction, so that the individual pixel size (called a "voxel" in three dimensions) is 12 μm horizontally, 47 μm vertically, and 2 μm axially, which gives a total of 512, 128, and 1024 voxels in each respective direction. The raw data produced by the SD-OCT instrument was imported into their proprietary software for analysis and reconstruction (Cirrus Research Browser, version 6.2.0.3, Carl Zeiss Meditec, Inc.) and exported to files describing the reflectivity measured at each voxel location with 8-bit precision (limit imposed by proprietary software). All the data processing and methods described here were later implemented and carried out using MATLAB (The MathWorks, Inc., Natick, MA, USA).

We defined three topographic regions of analysis as following the Early Treatment Diabetic Retinopathy Study (ETDRS) standard: *fovea*, defined as a circle with a 0.5-mm radius from the foveal center; *parafovea*, as a ring 0.5 to 1.5 mm distance from the foveal center; and *peripheral fovea*, as a ring 1.5 to 3.0 mm distance from the foveal center. For depth analysis, we defined *total retina* as bounded by the inner limiting membrane (ILM) and the outer border of the RPE; *inner retina* as bounded by the ILM and the inner nuclear layer (INL)–outer plexiform layer (OPL) junction; and *outer retina* as bounded by the INL-OPL junction and the outer border of the RPE. This avoids the variable thickening of OPL and Henle's layer in recordings.[9,10] Thickness measurements were automatically generated for each A-scan location (pixel location in an en face image). Regional thickness values were computed by averaging the measured values within each given topographic region and combining data from both patient eyes. An example displaying these analyses is shown in Figure 1.

Segmentation Technique and Computation of Thickness Maps

The axial depth of the ILM boundary, INL-OPL junction, and outer boundary of the RPE layer were determined automatically in all A-scan locations for all the SD-OCT volumes considered in this work using a segmentation algorithm our group has recently developed (de Sisternes L, et al. *IOVS* 2014;55;ARVO E-Abstract 4799; Leng T, et al. *IOVS* 2014;55;ARVO E-Abstract 4802). This tool automatically outlines the location of the mentioned boundaries (among others) within each axial scan in an SD-OCT volume using the voxel intensity values (brightness) and gradient magnitude (strength of a dark-to-bright or bright-to-dark transition), direction and orientation (discrimination between dark-to-bright or bright-to-dark transitions) in an iterative filtering process, together with a set of smoothing and anatomical constraints (order of appearance in the axial direction and the known constraint that the layers do not cross each other). The location of the center of the foveal

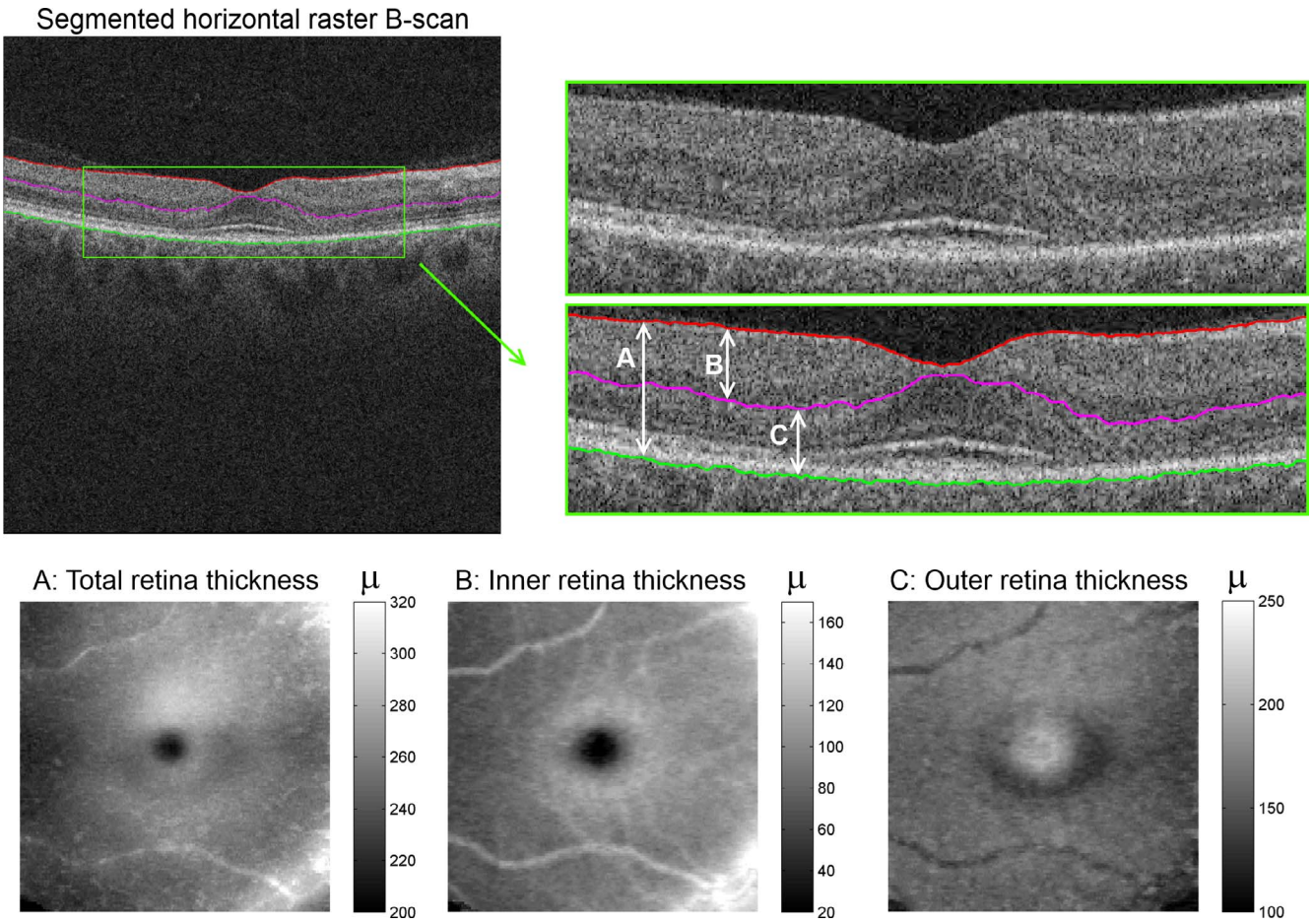

Figure 1. Example results from the automated processing of the data from a Cirrus SD-OCT scan of a right eye with moderate toxicity (M2). *Top*: Automatically segmented intraretinal layers in horizontal raster B-scan. The images on the *right* represent a detail of the B-scan on the *left* with and without the segmentation markings. *Labeled arrows* show the thickness of total retina (**A**), inner retina (**B**), and outer retina (**C**). *Bottom*: Topographic images showing total retina thickness, inner retina thickness, and outer retina thickness.

pit location also was determined automatically. Validation of the results produced by the segmentation technique is reported in the Results, and a brief description of the automated segmentation technique is included in the Appendix.

En face thickness maps for the total retina, inner retina, and outer retina are then determined by computing the axial differences between the corresponding segmented boundaries at each location in the horizontal-vertical plane. Figure 1 shows the segmentation result of a case of moderate toxicity (the right eye of case M2, which has parafoveal thinning and ellipsoid zone band loss, but no RPE damage) and the appearance of thickness maps. Note that the segmentation is pixel-by-pixel throughout the image, with no gap zones that might miss localized areas of pathology.

Computation of Progression Maps Over Time

Given the total, inner, and outer retina thickness maps, corresponding maps of thickness progression within given time intervals were computed by determining the slope of a linear fit over time of the recorded thickness values at each pixel location, considering those scans acquired within the time interval. To reduce variability in the progression maps due to noise in the scans and possible misalignments in the longitudinal images, the thickness maps were aligned with the center of the image corresponding to the center fovea pit location and filtered with a median filter with a circular kernel of 0.115-mm radius.

Results

Validation of Pixel-by-Pixel Automated Segmentation Results

Our goal was to examine the distribution and depth of HCQ damage between stages of retinopathy and as retinopathy progresses. Previous publications had used the ETDRS cube thickness measurements and the ganglion cell analysis of the Cirrus HD instrument for this purpose. However, although the Cirrus unit lets a user visualize topographic thickness images, it does not provide pixel-by-pixel topographic thickness measurements at high enough resolution for a detailed quantitative evaluation of changes over time. We also found in practice that the ganglion cell analysis (developed for glaucomatous eyes) placed boundaries incorrectly in many of our patients with HCQ retinopathy who had localized regions of outer retinal thinning. Figure 2 shows two examples of Cirrus ganglion cell analysis scans that would clearly cause erroneous thickness measurements if used to measure inner retinal changes with HCQ.

For these reasons, we used a Stanford pixel-by-pixel segmentation algorithm (see Methods and Appendix) to follow

Investigative Ophthalmology & Visual Science

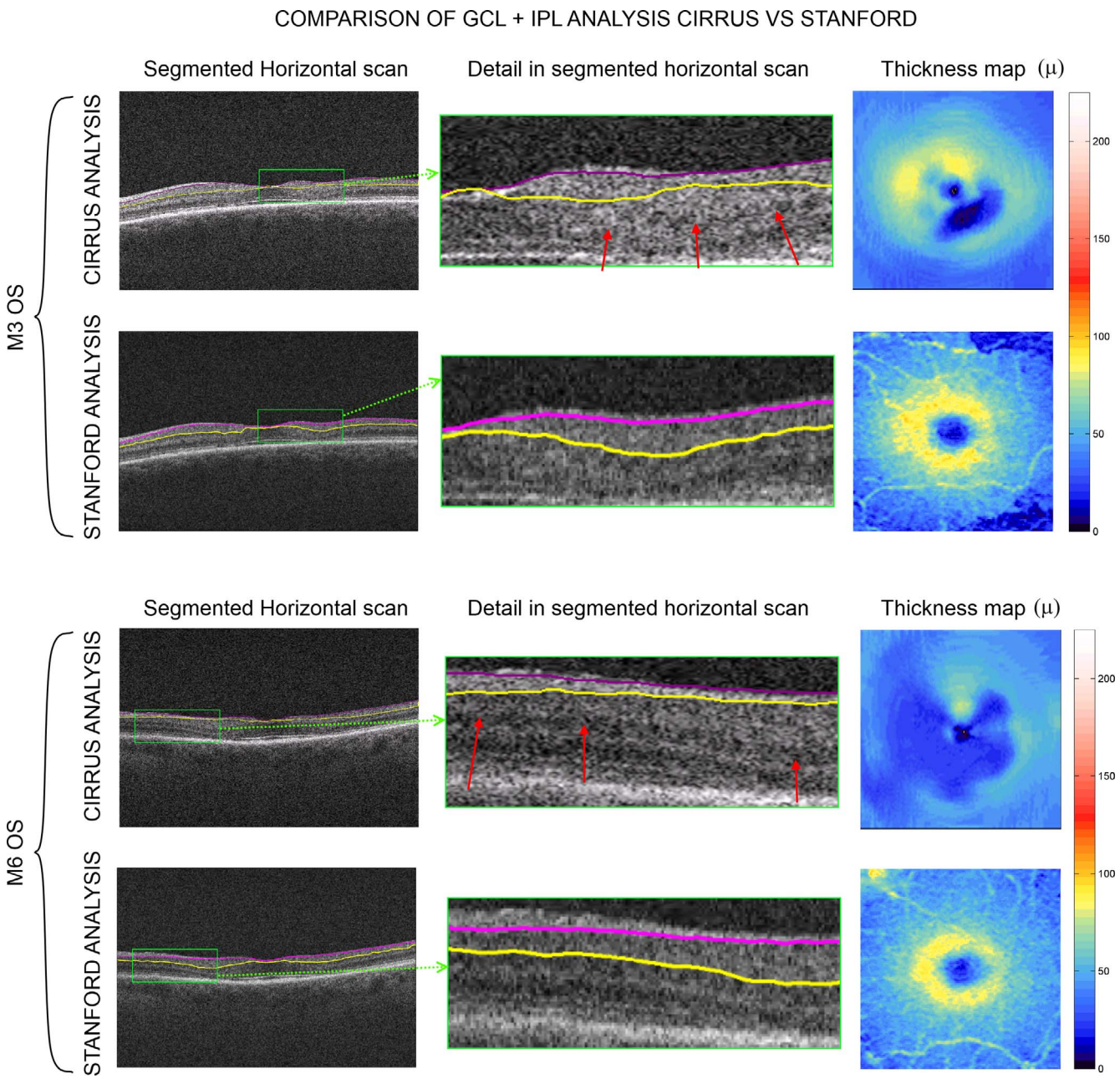

Figure 2. Comparison of inner retinal segmentation using the Cirrus system (labeled in the figure as Cirrus analysis) and our segmentation technique (labeled as Stanford analysis). Two eyes are shown, with moderate HCQ retinopathy and parafoveal thinning (M2 and M6 in the Table). The Cirrus system was designed to mark the *inner* edge of the ganglion cell layer in *magenta*, and the *outer* edge of the inner plexiform layer (IPL) in *yellow*. Regions of parafoveal thinning in the *green rectangles* are expanded in in the second column. *Red arrows* indicate where the outer edge of IPL was incorrectly placed by the Cirrus analysis, although the Stanford analysis marked these boundaries correctly. The topographic displays in the third column show topographic maps as processed by the Cirrus analysis and by the Stanford analysis. Regions of erroneous parafoveal thinning (*dark blue*) shown by the Cirrus analysis are not seen in the maps processed by the Stanford analysis.

inner and outer retinal deviations. This system also allowed us the manipulation of the topographic data to show regional damage and rates of change. Figure 2 shows that this program could correctly localize the retinal boundaries in the presence of HCQ retinopathy in example scans where the Cirrus analysis erred. To validate the automated thickness measurements for our cases, every SD-OCT scan (a total of 102 recordings) was assessed qualitatively by an expert ophthalmologist (MFM), to confirm segmentation of the retinal layers (which was accurate in all cases). This qualitative evaluation included the individual analysis of boundary positioning in both horizontal and vertical raster scans. Although this analysis does not necessarily validate the method for its general use and in the presence of other retinal diseases, it ensures the accuracy for the subjects in this report. This procedure also demonstrated consistency, as we had multiple recordings from the same subjects on return visits. Additionally, we compared total retina thickness values in the ETDRS regions as computed by our automated algorithm with those produced by Cirrus proprietary software (which is expected to be correct for total retinal thickness) and found less than 5% difference in these measurements for all eyes in the study.

Investigative Ophthalmology & Visual Science

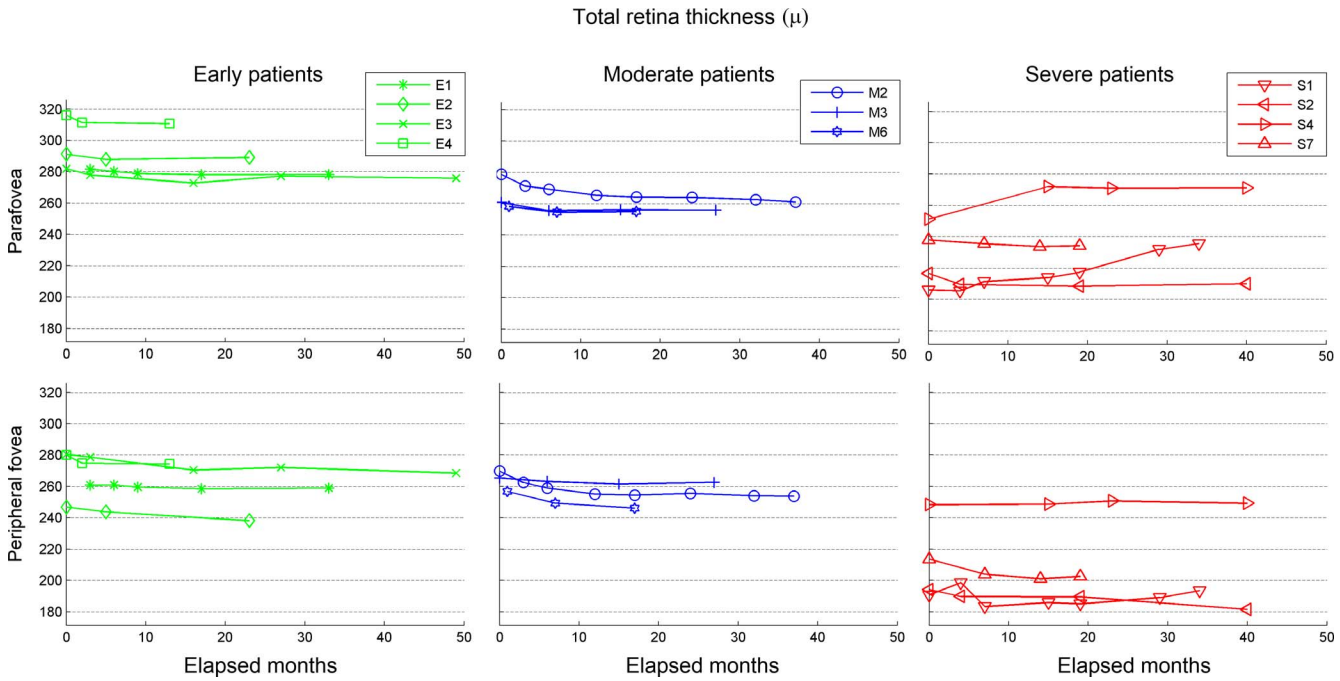

Figure 3. Total retina thickness measurements (microns) over time after HCQ had been stopped. Values for parafovea (*top row*) and the peripheral fovea (*bottom row*) are shown for early, moderate, and severe retinopathy patients. Measurements are averaged between both left and right eyes.

Retinal Thickness of Parafovea and Peripheral Fovea After Cessation of HCQ

Figure 3 shows change in full retinal thickness after HCQ was stopped. Measurements were averaged between both left and right eyes and across the designated parafovea and peripheral fovea regions, for all cases (early, moderate, and severe retinopathy). The early and moderate cases showed mild thinning in the parafoveal region (mostly less than 10 μm) during the first year, relative to baseline, after stopping the drug, as previously reported from clinical measurements.[5] However, there is similar thinning in the peripheral fovea, so that the progressive damage is not limited to the parafovea. Note that the parafoveal region is distinctly thinner in moderate patients than in early patients at the time that toxicity was recognized, whereas the thickness of the peripheral fovea is essentially the same. This suggests that the bull's-eye pattern of parafoveal thinning developed primarily between early and moderate stages of toxicity while using HCQ. In severe cases, the retina is thin in both regions, and there is little change with time as the photoreceptors are already severely damaged throughout them. Some severe eyes showed a degree of thickening, perhaps from RPE proliferation.

Figure 4 shows automated measurements of the thinnest point in the central foveal pit, as an index of foveal integrity. Data are averaged between both left and right eyes. We had previously reported foveal thickness measurements from the ETDRS cube,[5] but these data covered a region roughly 1 mm wide, and thus were influenced by the width of preserved foveal structures as much as the status of the foveolar center. Our segmentation program determines foveal thickness at the lowest smoothed point within the central region. The difference plots (Fig. 4, top) from early and moderate cases show only a small decrement of central thickness during the first year after stopping HCQ, whereas severe cases show dramatic thinning that continues for more than 3 years. The few points with increased thickness are within scan variability (<5 μm). These data confirm the previous conclusions with measurements at the actual foveal center. The absolute thickness measurements (Fig. 4, bottom) show only a small difference between early and moderate cases (the foveolar center is still relatively well preserved in both), whereas there is marked thinning at baseline in cases with severe disease.

Inner Versus Outer Retinal Thickness After Cessation of HCQ

Figure 5 illustrates thickness measurements obtained from the automated segmentation of inner and outer retinal layers, averaging the two eyes of each patient. Plots of change from baseline for early and moderate cases (Fig. 5A) show strikingly that the full-thickness thinning after stopping HCQ in Figure 3 came entirely from the outer retina. There was no change in inner retinal thickness with time in either parafovea or peripheral fovea. In contrast, there was prominent thinning of outer retina in moderate cases, and subtle thinning in early ones, during the first year after stopping the drug (but not thereafter). The absolute thickness plots (Fig. 5B) show not only that inner retina did not change with time (in all cases), but that the thickness of inner retina was very similar among all the cases, including the severe ones. In contrast, the outer retina is somewhat thinner in the parafovea of moderate cases than in early ones, but not in the peripheral fovea (as shown for full thickness in Fig. 3). This correlates with the development of bull's-eye thinning on SD-OCT. The outer retina of severe cases is much thinner than either early or moderate cases in all regions of the macula.

Topographic Changes Between Different Stages of Retinopathy (On the Drug)

Figure 6 compares the average thickness of retinal layers from early, moderate, and severe cases (averaging the two eyes, as well as the different patients in each category), measured while the patients were still using HCQ (at the time that retinopathy was first recognized). Each group represents a different set of

Investigative Ophthalmology & Visual Science

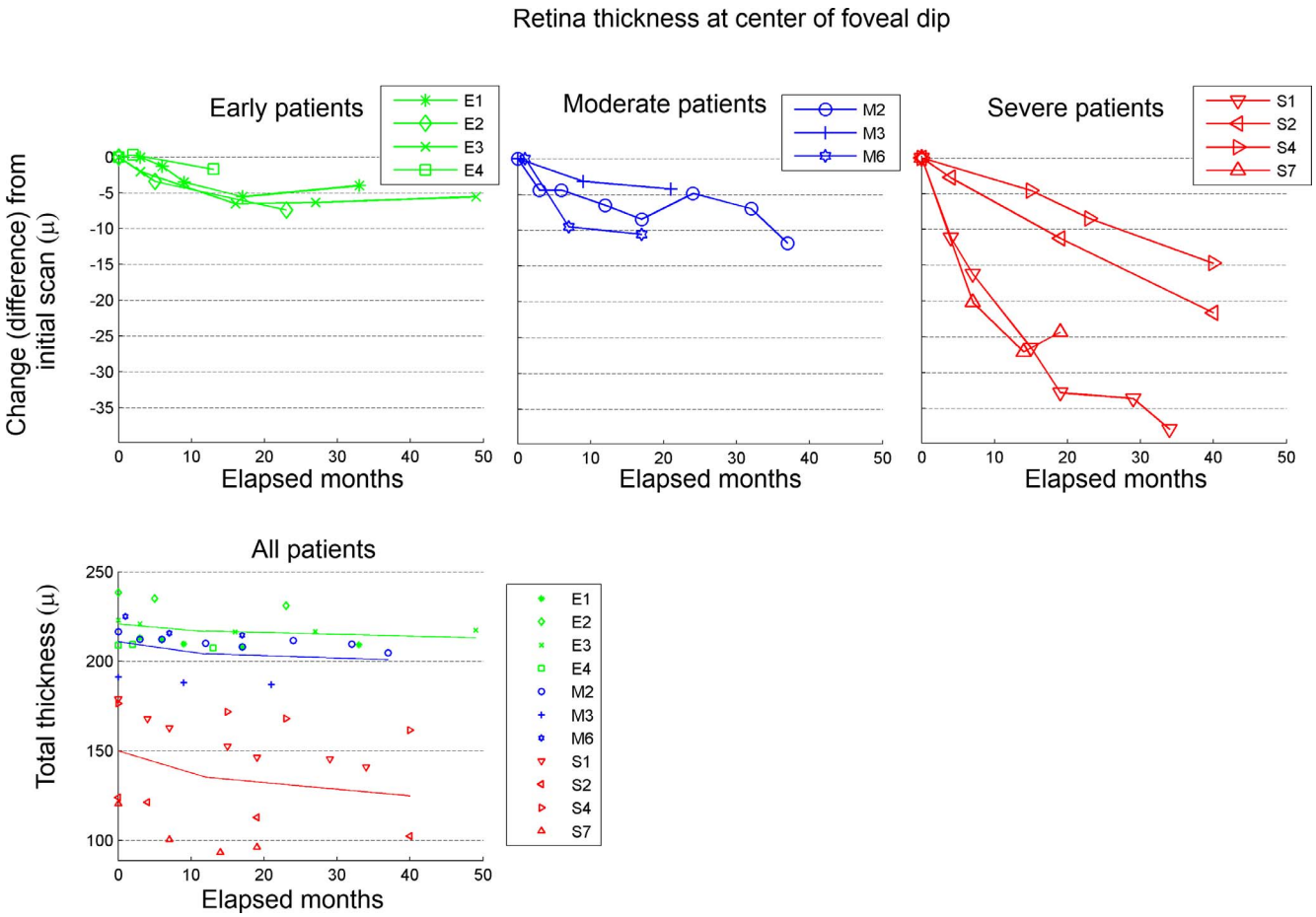

FIGURE 4. Foveolar thickness measurements at the center of the foveal pit, over time after stoppage of HCQ. Measurements are averaged between both left and right eyes. *Top row*: Difference from baseline (microns) for early (*left*), moderate (*middle*), and severe (*right*) retinopathy patients. *Bottom row*: Total retina thickness (microns) for all patients in the study. Lines show the average linear fit in each class, during the first year, and in later years.

patients (listed in the Table) so that there could be some individual variation in retinal thickness, but the analysis is useful nonetheless for showing major differences between the stages of retinopathy while the drug is being used. The color-coded topographic plots show the *difference* in thickness between early and moderate disease groups, and the d*ifference* between early and severe disease groups. This figure shows dramatically how toxicity progresses, while patients are taking HCQ, to drive the retinopathy through different stages of damage. Between early and moderate stages (Fig. 6, top row), there is clear development of parafoveal outer retinal thinning (bull's-eye pattern). However, the only change in inner retinal tissue is a rather faint ring of thinning (light blue color) that is mostly *outside* the dimensions of the bull's eye, and a bit of central thickening (yellow). In contrast, between the early and severe stages of damage (Fig. 6, bottom row), photoreceptors become markedly thinned across the entire macula, and this may obscure the bull's eye. Interestingly, the inner retinal thickness remains similar between our early and severe cases, and the ring of slight thinning visible in the moderate cases has disappeared. There is some irregular peripheral thickening that may represent RPE proliferation in such eyes.

Figure 7 suggests a possible explanation for the subtle inner retinal changes between early and moderate disease, given that inner retina must slide into parafoveal defects of the outer retina. The exaggerated diagram shows that as inner retina moves into an outer retinal defect, it tends to thin slightly at the outer edge of the photoreceptor damage and thicken slightly inside the damage zone, depending on the degree of sliding and settling. These changes would disappear when the photoreceptors become damaged diffusely as in many cases with severe disease.

Topographic Changes Over Time After HCQ Is Stopped

These same types of display can show temporal changes if toxicity progresses after HCQ is stopped. Figure 8 shows an exemplary case (M2, left eye) followed at 0, 6, 12, 24, and 37 months after cessation of the drug. The gray-scale plots show absolute thickness of the inner and outer retina, in which small differences are hard to discern. However, the color-coded difference plots (green = stability) show changes very clearly. Note that the figure shows changes from baseline (discovery of toxicity) to year 1, and then compares this change with what happened between the 1-year examination and the final examination at year 3. Note that inner retina was stable throughout the follow-up period in both parafovea and peripheral fovea. In contrast, outer retina showed diffuse thinning in the first year involving peripheral fovea as much as parafovea, but no further change between years 1 and 3.

Figure 9 shows the averaged difference maps of progression for all the early cases and all the moderate cases, respectively (and averaging the two eyes); that is, the continued progres-

Investigative Ophthalmology & Visual Science

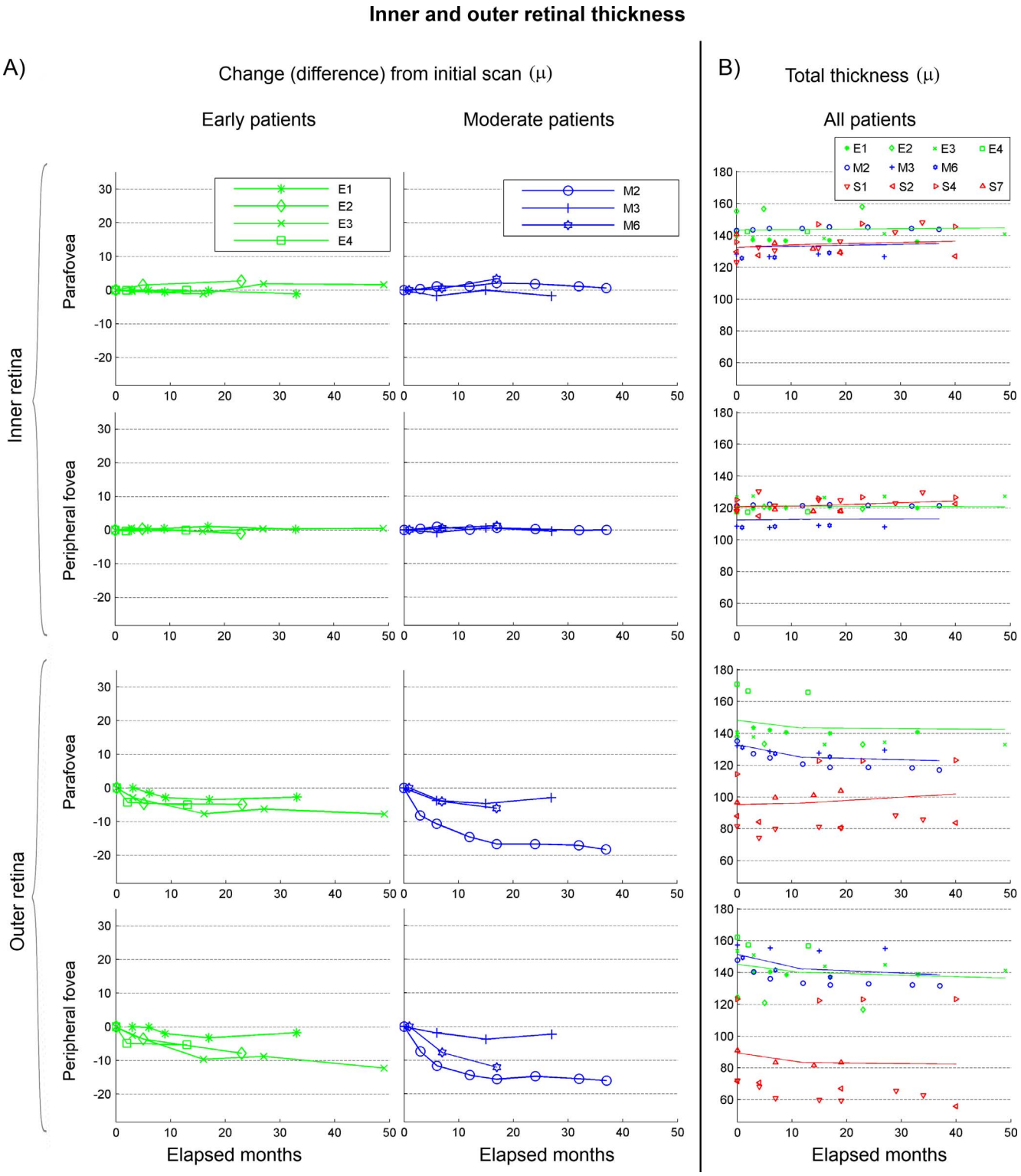

Figure 5. Inner and outer retinal thickness over time after stoppage of HCQ, comparing parafovea with peripheral fovea. Measurements are averaged between both left and right eyes. First and second columns (**A**) show difference from baseline for early and moderate cases; third column (**B**) shows absolute measurements from all patients. First two rows show inner retinal data; last two rows show outer retinal data. The lines in the third column show the average linear fit at each stage of disease, during the first year, and in later years.

sion of toxicity in cases that were designated as early or moderate at the time the drug was stopped. Figure 9 shows the change in inner and outer retinal thickness during the first year after stopping HCQ, and then the change between year 1 and the end of follow-up (at least 2 years from baseline). These images confirm that there is essentially no change in inner retinal thickness after drug cessation in either early or moderate cases. In contrast, the outer retina thins across the

Investigative Ophthalmology & Visual Science

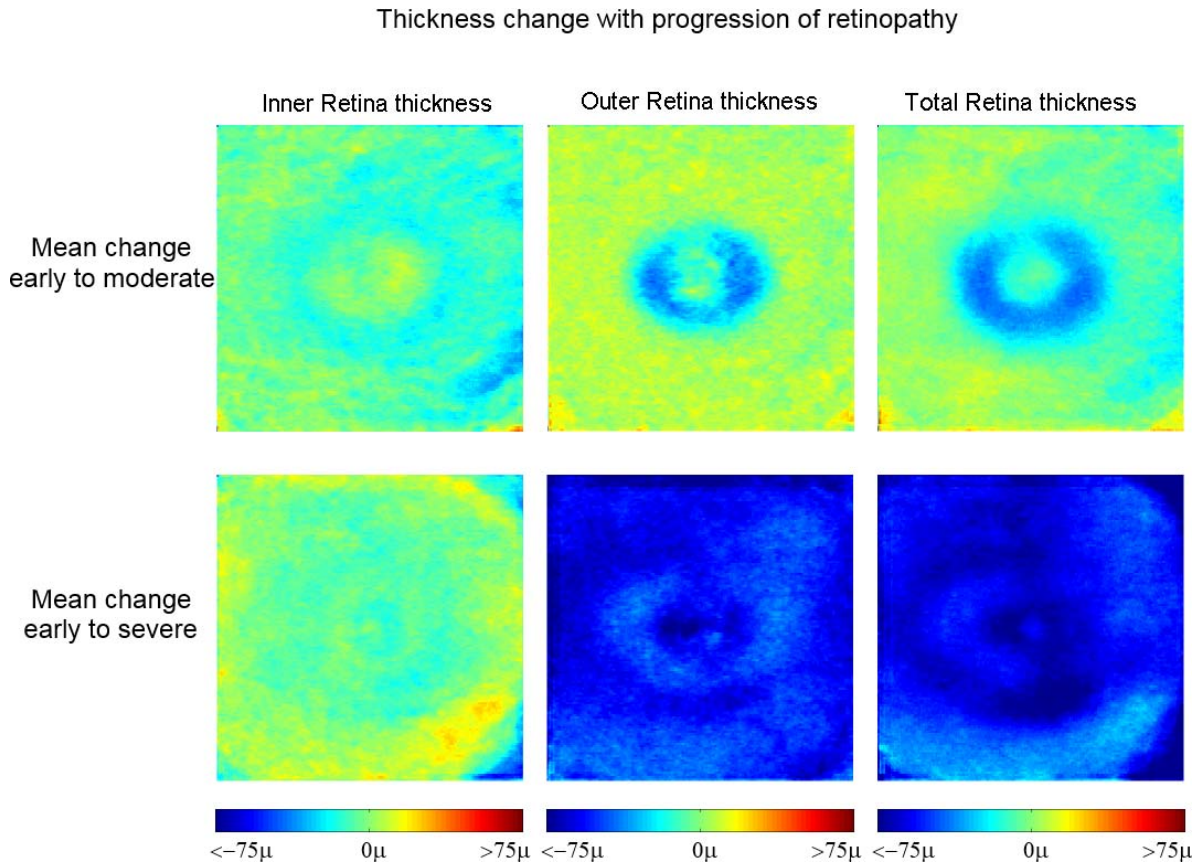

Figure 6. Topographic average thickness differences in different retinal layers between early and moderate eyes (*top*) and between early and severe eyes (*bottom*), averaging the two eyes, as well as the different patients in each category. *Blue* is thinning, *yellow* and *red* thickening, relative to early cases.

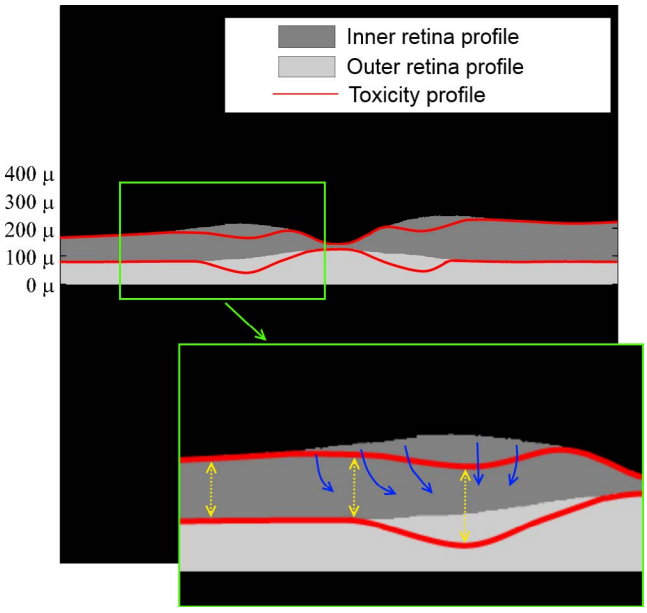

Figure 7. Illustrative (exaggerated) diagram explaining the inner retina thickness changes observed in Figure 6. The *blue arrows* illustrate the direction of inner retina movement to fill in outer retina loss. The *yellow arrows* indicate regions where inner retina thickness remains equal (*left*), shows thinning (*middle*), and shows thickening (*right*) relative to normal at that location (*dark gray*).

entire macula (i.e., without parafoveal localization) to a slight degree during the first year in early cases, and to a more prominent degree in moderate cases. We observed almost no progression in outer retinal thickness after the first year. The changes in total retinal thickness mirror the changes in outer retina.

Discussion

Our automated segmentation and topographic mapping has provided new information about the role of retinal layers and about the regional distribution of HCQ damage across the macula, as HCQ retinopathy progresses on or off the drug. The topographic maps show that HCQ toxicity localizes in the parafovea (bull's-eye distribution) as retinopathy evolves in patients using HCQ from an early to a moderate stage of damage, but this is followed by diffuse loss of photoreceptor cells (ONL) across much of the macula as damage becomes more severe. The analysis confirms our previous finding that when HCQ is stopped at an early or moderate stage (before RPE damage has occurred), there is progression only for approximately 1 year, in contrast to the long-term progression of damage that is seen in severe toxicity (with RPE involvement). However, the analysis showed that postdrug damage occurs diffusely across most of the macula (i.e., without parafoveal predilection), even in early cases where parafoveal thinning is not yet prominent. The results show that after the early development of localized damage, HCQ toxicity should be viewed as a largely diffuse maculopathy. Studies on

Investigative Ophthalmology & Visual Science

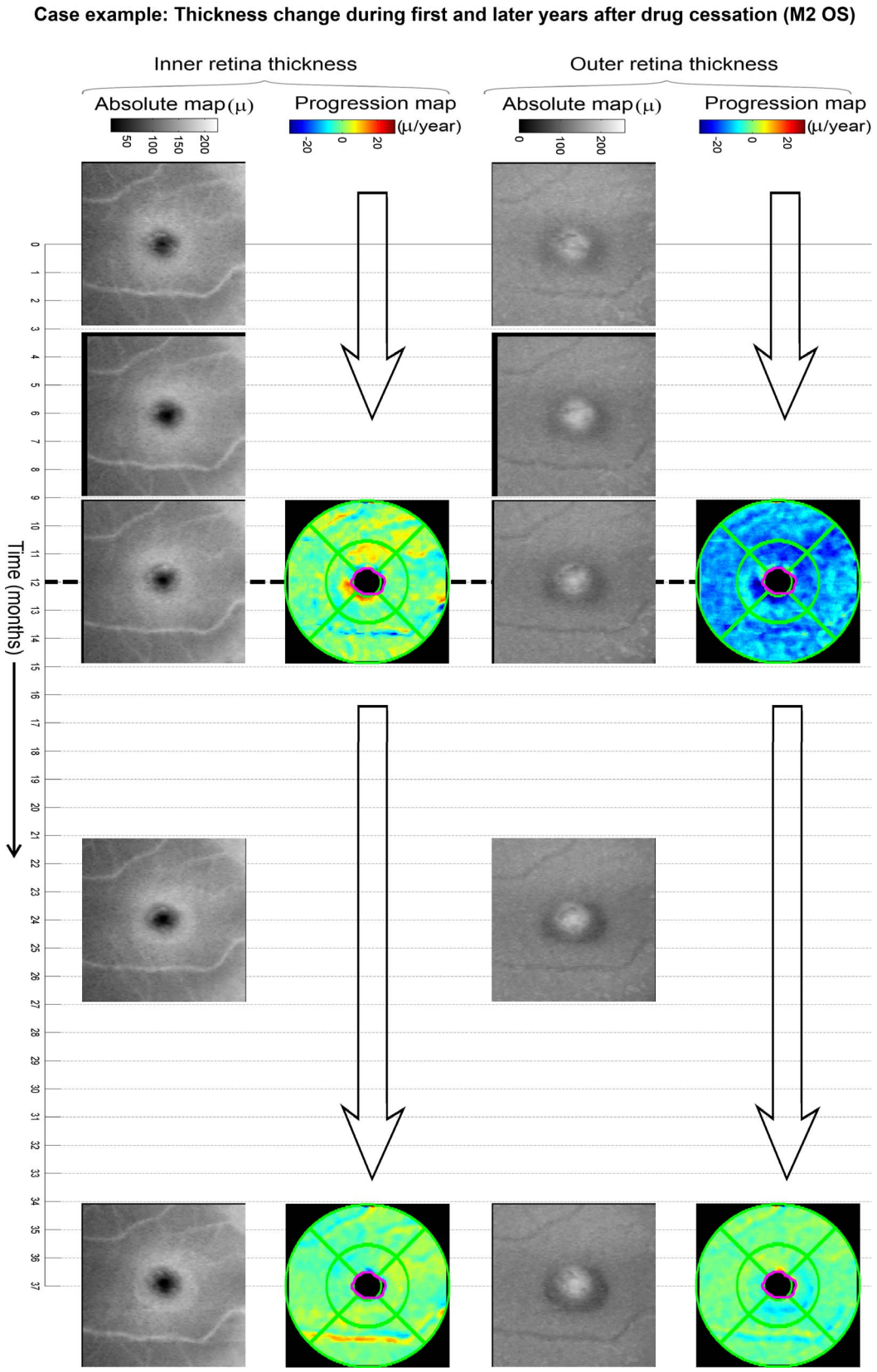

Figure 8. Topographic analysis of inner and outer retinal thickness after stopping HCQ. The figure compares inner retinal (*left*) and outer retinal (*right*) thickness maps from the left eye of a patient with moderate toxicity over 37 months after stopping HCQ. The vertical axis indicates months elapsed and each thickness map is centered at the time it was acquired. The colored progression difference maps show the change from baseline to 1 year, and then from 1 year onward. The only significant change was diffuse outer retinal thinning in the first year.

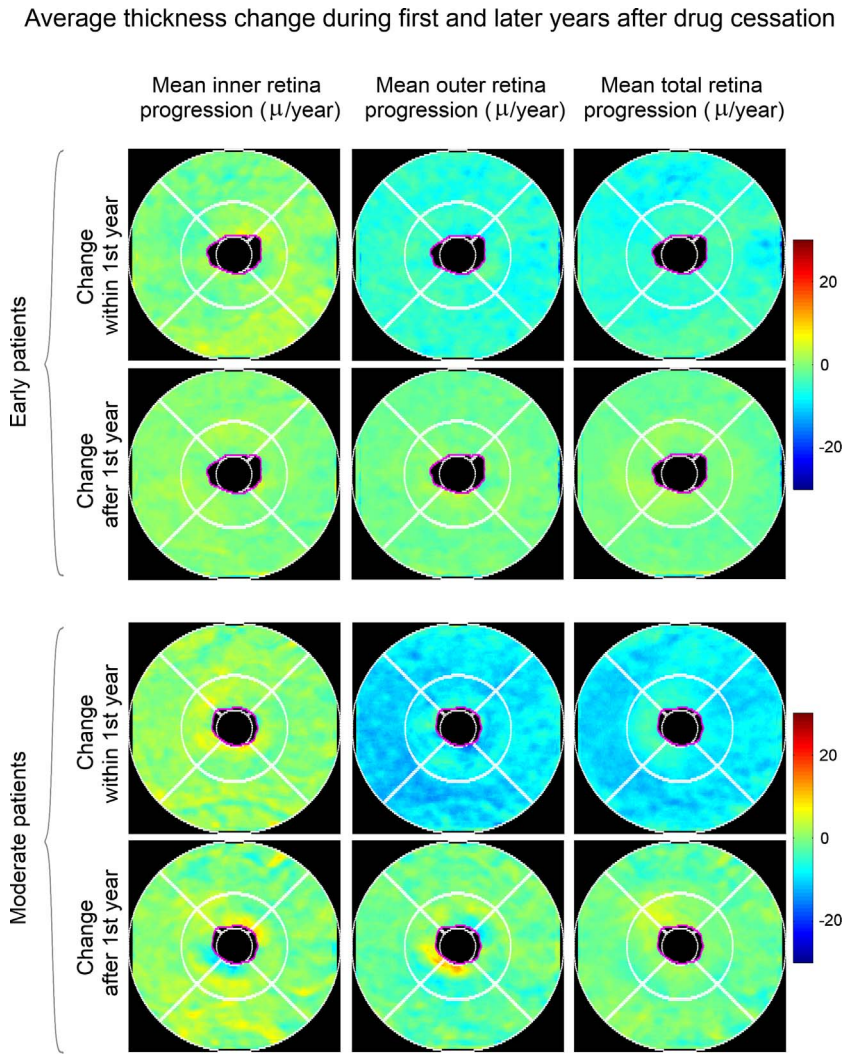

Figure 9. Average progression of inner, outer, and total retinal thickness (*left to right columns*), comparing data from early patients (*top two rows*) and moderate patients (*bottom two rows*). For each stage of retinopathy, the *top row* shows progression during the first year after stopping the drug, and the *second row* shows progression from year 1 to the final examination. Maps show data averaged between the two eyes.

the full-field ERG show that signals are usually normal even in the presence of moderate maculopathy, but the ERG is definitely reduced in many cases of "severe" retinopathy where the entire macula is thin.[3]

All of our measurements of segmented retina showed that retinal thinning from HCQ toxicity was primarily a result of outer retinal damage. There was virtually no change in inner retinal thickness in our patients between different stages of retinopathy, and no inner retinal thinning was observed with time after stoppage of the drug. Because we have only a small number of patients in each category of retinopathy, we cannot rule out the possibility of minor or subtle inner retinal loss between early, moderate, and severe stages of retinopathy. On the other hand, if inner retinal damage was progressing in concert with outer retinal damage, this should have been evident in our patients who were followed for several years.

Some previous publications showed small changes in inner retinal thickness (in the general range of 5 μm), localized inferiorly, or in the parafovea or peripheral fovea.[6–8] However, these measurements were derived from commercial ganglion cell layer analyses that are designed primarily for glaucoma[11] and do not always conform to focal areas of outer retinal pathology. Figure 2 showed two examples in which Cirrus ganglion cell layer segmentation has erred in estimating inner damage above a region of parafoveal outer retinal thinning. The segmentation method we used here avoided such errors. Furthermore, the observations of inner retinal thinning in previous studies may in part reflect local distortion (see Fig. 7) rather than a loss of neural substance. In our study, this distortion effect disappeared when retinopathy became more severe and the retinal thinning was widespread. Our data suggest that inner retina is neither a major target of HCQ toxicity, nor is it likely to be useful as a screening tool for toxicity.

A more recent study by Lee et al.,[12] based on Cirrus ganglion cell segmentation, found little correlation between inner retinal thickness and HCQ exposure among nontoxic patients, which supports our findings. However, a few of their patients with toxicity showed severe thinning of the inner retina in direct contrast with our results. Some of this could represent segmentation errors, as in Figure 2, or be idiosyncratic or from other disease (they also had one nontoxic patient with marked thinning). Lee et al.[12] studied Asian patients, who often show HCQ damage in a more peripheral pattern,[2] whereas our patients had predominately parafoveal damage. It is conceivable that some conclusions about inner

retina could differ with ethnic origin, although our inner retinal analysis covered a similar extent as the Cirrus analysis used by Lee et al.[12]

From a practical standpoint of patient management, most patients are not aware of mild paracentral scotomas from early HCQ toxicity. Thus, the clinical concern that drives screening is not the prevention of mild off-center scotomas, but the prevention of central visual loss (which is determined by foveolar damage). Our topographic data show the degree of central foveal damage more precisely than our previous study,[5] and confirm that cases recognized at an early and moderate stage (before RPE damage) do not lose major foveal thickness after HCQ is stopped (as occurs with retinopathy that shows RPE damage). This emphasizes the importance of regular screening[13] and the importance of new recommendations for dose management to reduce the risk of toxicity.[1] Automated analysis in SD-OCT images aimed to visualize and analyze toxicity en face and pixel-by-pixel are potentially useful tools to quantify and identify early signs of maculopathy, in a similar manner as they have already shown potential in finding predictors for the transformation of dry to wet AMD.[14]

In conclusion, our pixel-by-pixel analysis of topographic SD-OCT data shows that HCQ toxicity primarily involves only the outer retina. The initial damage to the retina while patients are taking HCQ is in the parafoveal region, but as toxicity progresses (and also after the drug is stopped) the damage is better described as a diffuse maculopathy. We confirm that detection of retinopathy at an early or moderate stage (before RPE damage) effectively limits postdrug progression and prevents major foveal damage. These data add to understanding of how HCQ toxicity develops, and reinforce the importance of regular screening to detect retinopathy at an early stage.

Appendix

Intraretinal Layer Segmentation in SD-OCT Images

The segmentation algorithm automatically outlines the axial location of intraretinal layer boundaries within the three-dimensional (3D) SD-OCT data, using image intensity and gradient properties in an iterative filtering process, wherein a set of smoothness constraints and predefined rules are considered. The key elements of the method used are shown in Figure A1, together with example results for the segmentation of the ILM, inner and outer boundaries of the INL, and outer boundary of the RPE. The algorithm is based on an iterative process that updates the segmentation to closely follow the actual location of each boundary while maintaining a smooth behavior. At each step in the iterative process, the results from the previous iteration step are refined using a weighted median filter adapted for the 3D SD-OCT cubes, while also considering smoothness and anatomical constrains that are common to every eye (order of appearance of the layers in the axial direction and the known constraint that the layers do not cross each other). This process seeks to resolve axial boundaries with smooth behavior topographically while the defined weights favor locations with stronger transitions with similar axial orientation. The iterative process stops once it finds a stable converging solution for the localization of each boundary. The initial estimations of each boundary axial location, acting as seed for the iterative process, are determined A-scan by A-scan, considering intensity and 3D gradient statistics within the SD-OCT cube as well as the anatomical constrains.

The weighted median filtering process governing the iterations is defined in the following way: at each iteration k, the axial (depth) location in the (x,y) coordinates (in the horizontal and vertical axes, respectively) of the retinal boundary, $B(x,y)^k$, are updated given the results from the last iteration $B(\mathrm{X},\mathrm{Y})^{k-1}$, with (X,Y) indicating the subspace defined by the cube horizontal-vertical extent,

$$B(x,y)^k = \underset{\theta}{\operatorname{argmin}} \sum_{n=-L}^{L}\sum_{m=-L}^{L} W\Big(x,y,B(x+n,y+m)^{k-1} - S(x+n,y+n;\beta)^{k-1} + S(x,y;\beta)^{k-1}\Big)^{k-1} \cdot \Big|\Big(B(x+n,y+m)^{k-1} - S(x+n,y+n;\beta)^{k-1} + S(x,y;\beta)^{k-1}\Big) - \theta\Big|$$

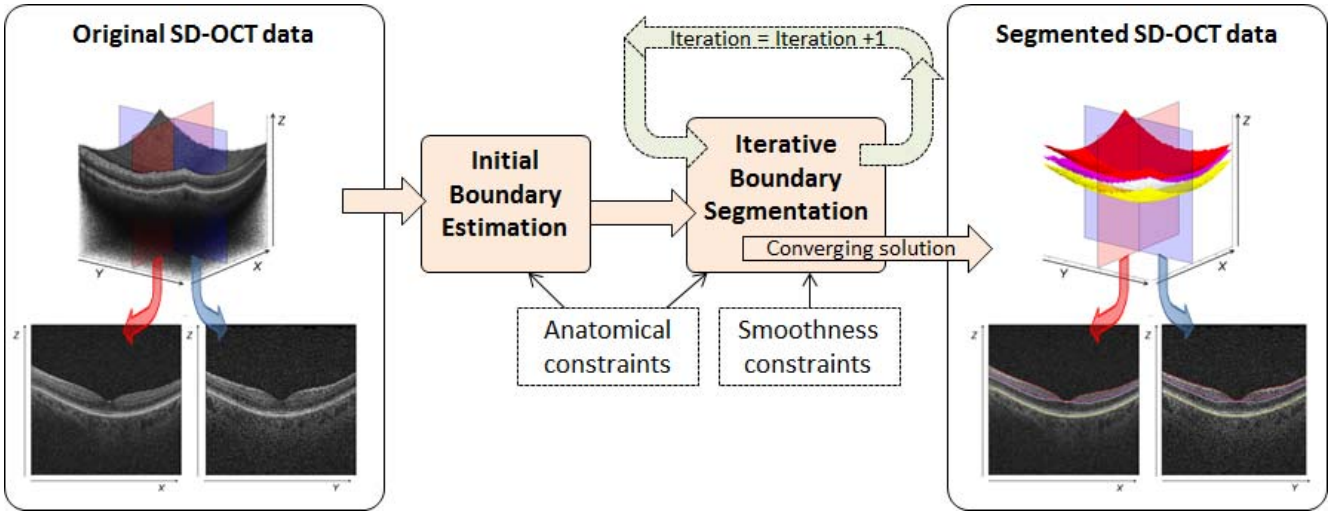

Figure A1. Key elements in the segmentation algorithm. The images shown in the original SD-OCT data box include a 3D representation of an example SD-OCT cube (*on top*) and the horizontal and vertical scans across the macula center (with locations within the cube indicated by the *red* and *blue planes*, respectively). The images shown as segmented SD-OCT data include a 3D representation of the axial location of the segmented ILM, inner and outer boundaries of the INL, and outer boundary of the RPE (*on top*) and horizontal and vertical scans across the macula center also displaying the segmented outlines (with locations within the cube indicated by the *red* and *blue planes*, respectively).

Investigative Ophthalmology & Visual Science

where $S(x,y;\ \beta)^{k-1}$ is a smoothing offset function, with a defined smoothing factor β. The weighting function $W(x,y,z)^{k-1}$ is defined in three dimensions in the following manner:

$$W(x,y,z)^k = r\left(\alpha \cdot |\nabla \mathrm{I}(x,y,z)| \cdot sgn\left(\frac{\partial \mathrm{I}}{\partial X}(x,y,z)\right)\right) \cdot M(x,y,z)^k,$$

where $\mathrm{I}(x,y,z)$ refers to the SD-OCT voxel value in the horizontal, vertical, and axial coordinates. The parameter α is set to indicate whether the boundary should present an increase in reflectivity in the axial direction (dark-to-light transition, with $\alpha = +1$), or a decrease in reflectivity (light-to-dark transition, with $\alpha = -1$). A masking volume $M(x,y,z)^k$ indicates the anatomical constraints within the retinal boundary and is set with a value of 1 for the voxels within defined upper and lower boundary limits in the axial direction and 0 otherwise; ∇ indicates a 3D gradient operator, $sgn(t)$ is the *signum* function, and $r(v)$ is the ramp function, defined as:

$$r(v) = \begin{cases} t, \text{ if } t \geq 0 \\ 0, \text{ if } v < 0 \end{cases}.$$

Automated Determination of Fovea Center in SD-OCT Images

The center fovea pit location is determined by finding the location with lowest total retinal thickness within the fovea pit region. The approximated topographic extent (extent in the horizontal-vertical plane) of the foveal pit is generated following a series of thresholding and morphological operations: We first applied a k-means classification algorithm[15] to the pixel-by-pixel topographic thickness measurements between the ILM and the outer boundary of the INL, dividing the values in two different groups. Values under the identified threshold by the k-means algorithm and within 1 mm to the center of the image were selected as initial mask estimation. We then applied a morphological opening to this mask followed by a morphological dilation with a kernel consisting on a circle of 0.25 mm radius. The location with minimum total retina thickness within the topographic locations included in this foveal pit mask was selected as the center.

Acknowledgments

The authors thank Ryan Nelson, BS (Byers Eye Institute), for his help in extracting the SD-OCT data analyzed in this work.

Supported by a Spectrum-SPADA innovation grant of Stanford University. Spectrum-SPADA is part of the Clinical and Translational Science Award program, funded by the National Center for Advancing Translational Sciences (Grant UL1 TR001085) at the National Institutes of Health. Publication supported by a research award from Retina Research Foundation and the Retina Society (MFM). The funding organizations had no role in the design or conduct of this research. The authors alone are responsible for the content and the writing of the paper.

Disclosure: **L. de Sisternes**, None; **J. Hu**, None; **D.L. Rubin**, None; **M.F. Marmor**, None

References

1. Melles RB, Marmor MF. The risk of toxic retinopathy in patients on long-term hydroxychloroquine therapy. *JAMA Ophthalmol*. 2014;132:1453–1460.
2. Melles RB, Marmor MF. Pericentral retinopathy and racial differences in hydroxychloroquine toxicity. *Ophthalmol*. 2015;122:110–116.
3. Marmor MF. Comparison of screening procedures in hydroxychloroquine toxicity. *Arch Ophthalmol*. 2012;130:461–469.
4. Rosenthal ARR, Kolb H, Bergsma D, Huxsoll D, Hopkins JL. Chloroquine retinopathy in the rhesus monkey. *Invest Ophthalmol Vis Sci*. 1978;17:1158–1175.
5. Marmor MF, Hu J. Effect of disease stage on progression of hydroxychloroquine retinopathy. *JAMA Ophthalmol*. 2014; 132:1105–1112.
6. Pasadhika S, Fishman GA. Effects of chronic exposure to hydroxychloroquine or chloroquine on inner retinal structures. *Eye*. 2010;24:340–346.
7. Pasadhika S, Fishman GA, Choi D, Shahidi M. Selective thinning of the perifoveal inner retina as an early sign of hydroxychloroquine toxicity. *Eye*. 2010;24:756–762.
8. Ulviye Y, Betul T, Nur TH, Selda C. Spectral domain optical coherence tomography for early detection of retinal alterations in patients using hydroxychloroquine. *Indian J Ophthalmol*. 2013;61:168–171.
9. Lujan BJ, Roorda A, Knighton RW, Carroll J. Revealing Henle's fiber layer using spectral domain optical coherence tomography. *Invest Ophthalmol Vis Sci*. 2011;52:1486–1492.
10. Ouyang Y, Walsh AC, Keane PA, Heussen FM, Pappuru RK, Sadda SR. Different phenotypes of the appearance of the outer plexiform layer on optical coherence tomography. *Graefes Arch Clin Exp Ophthalmol*. 2013;10:2311–2317.
11. Mwanza JC, Durbin MK, Budenz DL, et al. Glaucoma diagnostic accuracy of ganglion cell-inner plexiform layer thickness: comparison with nerve fiber layer and optic nerve head. *Ophthalmol*. 2012;119:1151–1158.
12. Lee MG, Kim SJ, Ham DI, et al. Macular retinal ganglion cell-inner plexiform layer thickness in patients on hydroxychloroquine therapy. *Invest Ophthalmol Vis Sci*. 2014;56:396–402.
13. Marmor MF, Kellner U, Lai TY, et al. American Academy of Ophthalmology Update Revised recommendations on screening for chloroquine and hydroxychloroquine retinopathy. *Ophthalmol*. 2011;118:415–422.
14. de Sisternes L, Simon N, Tibshirani R, Leng T, Rubin DL. Quantitative SD-OCT imaging biomarkers as indicators of age-related macular degeneration progression. *Invest Ophthalmol Vis Sci*. 2014;55:7093–7103.
15. Hartigan JA, Wong MA. A K-means clustering algorithm. *J R Stat Soc Series C*. 1979;28:100–108.